Airflow induced by pumping tests in unconfined aquifer with a low-permeability cap

Jiu Jimmy Jiao[1] and Haipeng Guo[1,2]

Received 21 January 2009; revised 15 July 2009; accepted 5 August 2009; published 31 October 2009.

[1] Most analytical and numerical models developed to analyze pumping test data focus on saturated flow below the water table. Traditionally the soil above the initial water table prior to pumping has been thought to have little influence on the test results and has usually been ignored. It is hypothesized that, if the unsaturated zone is capped by low-permeability soil, airflow in the unsaturated zone may be developed during pumping and may have impact on the drawdown in the aquifer. A transient, three-dimensional and variably saturated flow model is employed to simulate the pumping-induced air and groundwater flows in both the saturated zone and unsaturated zone with a low-permeability layer. The results demonstrate that negative pressure in the unsaturated zone can be generated by pumping. The negative pressure begins to appear as the drawdown rate increases to a maximum, approaches a peak before the drawdown rate becomes zero, and then gradually disappears. Drawdown obtained from the capped aquifer is much greater because the water in the pores in the unsaturated zone is sucked by the negative pressure and the gravity drainage from the pores is hampered. Consequently, the drawdown versus time curve does not conform to the traditional S-shaped curve for an unconfined aquifer but is similar to that of a confined aquifer. If the airflow caused by the low-permeability cap is ignored, the error in estimated drawdown could be over 80% for the specific parameters and aquifer configuration used in the study. The possible errors in parameter estimation when airflow is ignored are explored. Overall, the hydraulic conductivity of the aquifer can be overestimated and the specific yield of the aquifer underestimated if airflow is ignored. The estimation error for specific yield tends to be greater than that in hydraulic conductivity.

Citation: Jiao, J. J., and H. Guo (2009), Airflow induced by pumping tests in unconfined aquifer with a low-permeability cap, *Water Resour. Res.*, *45*, W10445, doi:10.1029/2009WR007760.

1. Introduction

[2] Pumping tests have proved to be one of the most effective ways of obtaining aquifer parameters. A test interpretation can be made using various analytical models based on simplified assumptions. The equation for unsteady state flow toward a well in a confined aquifer was established by *Theis* [1935]. In subsequent decades, analytical models were developed for pumping of different types of aquifers such as leaky and unconfined aquifers [e.g., *Boulton*, 1954; *Neuman*, 1972, 1974; *Moench*, 1995]. The concept of delayed water table response, which was pioneered by Boulton and significantly advanced by Neuman, was widely used to analyze the water table behavior in unconfined aquifers. Three distinct segments in S-shaped time-drawdown curves under water table conditions can be identified: the first segment represents instantaneous release of water from storage for a short period after pumping, the second segment is dominated by the effects of gravity drainage, and the third segment closely conforms with the Thesis curve when gravity drainage diminishes with time [*Boulton*, 1954; *Neuman*, 1972, 1974]. Various aspects of these models and limitations of the assumptions have been widely discussed. For example, *Moench* [2004] believed that traditional models do not adequately address effects of time-varying drainage from the vadose zone; Based on field test results, *Endres et al.* [2007] concluded that the delayed drainage models significantly overestimated the cumulative drainage flux and underestimated the undrained storage determined from the field data.

[3] Most of the models discussed above focus on saturated flow below the water table and traditionally the soil above the initial water table prior to pumping has been thought to have little influence on the test results and has usually been ignored. *Mathias and Butler* [2006] obtained a new drainage function based on a linearized Richards' equation assuming that moisture content and hydraulic conductivity are exponential functions of pressure head. *Tartakovsky and Neuman* [2007] developed a new analytical solution for the delayed response process characterizing flow to a partially penetrating well in an unconfined aquifer by accounting for unsaturated flow above the water table. They concluded that in typical cases, unsaturated flow does not have appreciable impact on early and late dimensionless time drawdown. *Moench* [2008] presented analytical and

[1]Department of Earth Sciences, University of Hong Kong, Hong Kong, China.
[2]China Institute of Geo-Environmental Monitoring, Beijing, China.

0043-1397/09/2009WR007760$09.00

numerical analyses of an unconfined aquifer test considering unsaturated zone characteristics and concluded that field-scale relative hydraulic conductivity declines more rapidly with elevation above the top of the capillary fringe than would be expected if the parameters were to be based on core-scale measurements and analyses. A review of the literature shows that there is one aspect which has not been addressed: the possible airflow induced by water pumping in unconfined aquifers and its potential impact on water level prediction and parameter estimation.

[4] Although there is little study of pump-induced airflow, general air or air-water flows and their interaction in unsaturated zones have been studied widely mainly in the fields of infiltration in vadose zones [*Peck*, 1965; *Touma and Vauclin*, 1986; *Linden and Dixon*, 1973; *Celia and Binning*, 1992; *Guo and Jiao*, 2008]. The air-water two-phase flow model should be used when the interaction between the air and water flows is significant, which is more realistic than single-phase air or water flow. *Linden and Dixon* [1973] conducted several field experiments to investigate infiltration and water table responses to soil air pressure under border irrigation, and observed that the water table was depressed at the center of the field and raised near the border strip. Rain infiltration can cause the so-called Lisse effect: the water-level increase in a well driven by airflow induced by an advancing wetting front during intensive rains [*Weeks*, 2002; *Guo et al.*, 2008]. When the air pressure is sufficiently high, however, air will escape from the soil surface, thereby causing a sharp decrease in air pressure and a major increase in the rate of infiltration [*Touma et al.*, 1984]. The concept that air pressure impacts water pressure has been used to design a pneumatic slug test, in which air pressure is used to displace/lower the water level and the change of water level is then recorded to estimate the aquifer hydraulic conductivity [*Zurbuchen et al.*, 2002].

[5] At the Hong Kong International Airport, over 100 dome-shaped heaves with diameters of 2–10 m were observed during heavy rain periods in 2000 (W. K. Leung et al., Heaving of airfield pavement at Hong Kong International Airport, paper presented at 2007 FAA Worldwide Airport Technology Transfer Conference, Atlantic City, 2007). The heave problem was mitigated when air pressure relief holes were installed. The first author was fascinated by this unusual phenomenon and initiated a study of tide-induced airflow [*Jiao and Li*, 2004; *Li and Jiao*, 2005; *Guo and Jiao*, 2008]. Using TOUGH2 [*Pruess et al.*, 1999], the two-phase air-water flow in unsaturated and saturated zones was simulated successfully to reproduce the observed air pressure [*Jiao and Li*, 2004]. When the water table rises, the air pressure in the unsaturated zone increases, the air is pushed to escape from the ground surface, and the ground surface "exhales." When the water table falls, the process is reversed and the ground surface "inhales." Abnormally high and low subsurface air pressure can be generated when the aquifer structure, rainfall, and fluctuation rate of sea level are favorably combined [*Jiao and Li*, 2004]. An analytical solution for one-dimensional airflow in an unsaturated zone induced by tidal fluctuation in a coastal two-layered system was developed based on several model simplifications [*Li and Jiao*, 2005]. This analytical solution was used to estimate air permeability of the marine sand fill at a coastal reclamation area.

[6] The first author speculates that pumping may also induce significant air pressure if the tide fluctuation and wetting front can generate appreciable air movement [*Jiao and Li*, 2004; *Weeks*, 2002]. The fluctuation rate of sea tide is usually <0.5 m/h, but pumping can cause the falling of water level at the rate of few meters per hour. Obvious airflow in an observation well during a major pumping test in Xiaolangdi, located in the Yellow River plain, China was noticed (L. Wan, personal communication, 2003). During the test, a sketchy paper being used to record the water-level data was almost sucked into the observation well and noise of airflow in the wellbore was heard. The site has a two-layered structure typical of river plains: a sandy channel deposit below a less permeable clayey overbank deposit. The initial water level was located immediately below the contact of the two layers (L. Wan, Water-supply study in the river plain located downstream of Xiaolangdi dam, Yellow River, China, unpublished manuscript, 2000).

[7] A less permeable layer above the main aquifer is not a uncommon scenario for pumping test sites, especially for those in river plain. The hydraulic conductivity of the soil above the initial table is believed to have no effect on the time-drawdown curve in traditional pumping test analysis. This may be different if airflow is considered. In this paper, a numerical study of two-phase air-water flow induced by pumping was conducted with TOUGH2 to test the hypothesis. The impact of airflow on drawdown of hydraulic heads in the aquifer was also explored.

2. Setup of the Numerical Model

2.1. Domain Description

[8] Figure 1 is a schematic depiction of the geometry and boundary conditions for the three-dimensional numerical model. The configuration and some key parameters of the aquifer system are based on the field test site in Xiaolangdi (Wan, unpublished manuscript, 2000). The origin of the system is the point where z and r axes meet. A soil cylinder with a thickness of 20 m is used as the model domain. The initial thickness of the saturated zone in the model, i.e., the aquifer, is set to be 17 m, thus the water table is 3 m below land surface. A partially screened pumping well with a radius of 0.15 m, screened below the water table, is located at the center of the domain. The screen length is 2.4 m and the bottom of the screen is 0.4 m above the impermeable bottom. The external radius of the domain is set to be 5000 m, which is sufficiently away from the pumping well so that the cone of depression cannot reach it during the pumping time. The uppermost nodes in the model are set to be the atmosphere boundary with a fixed air pressure equivalent to a water column height of 10.3 m. The unscreened part of the well wall, outer vertical boundary and base of the model are represented by a no-flow boundary.

[9] The background aquifer has a permeability of K. The system is air-confined if the soil near the ground surface has a low permeability of K_U [*Guo and Jiao*, 2008]. Various cases with different hydraulic conductivity combinations will be discussed. In the base case, the upper layer has a K_U of 5.54×10^{-8} m/s and a thickness (d_U) of 2.4 m, and the pumping rate is set to be 2500 m^3/day. Other parameters in the base case are shown in Table 1.

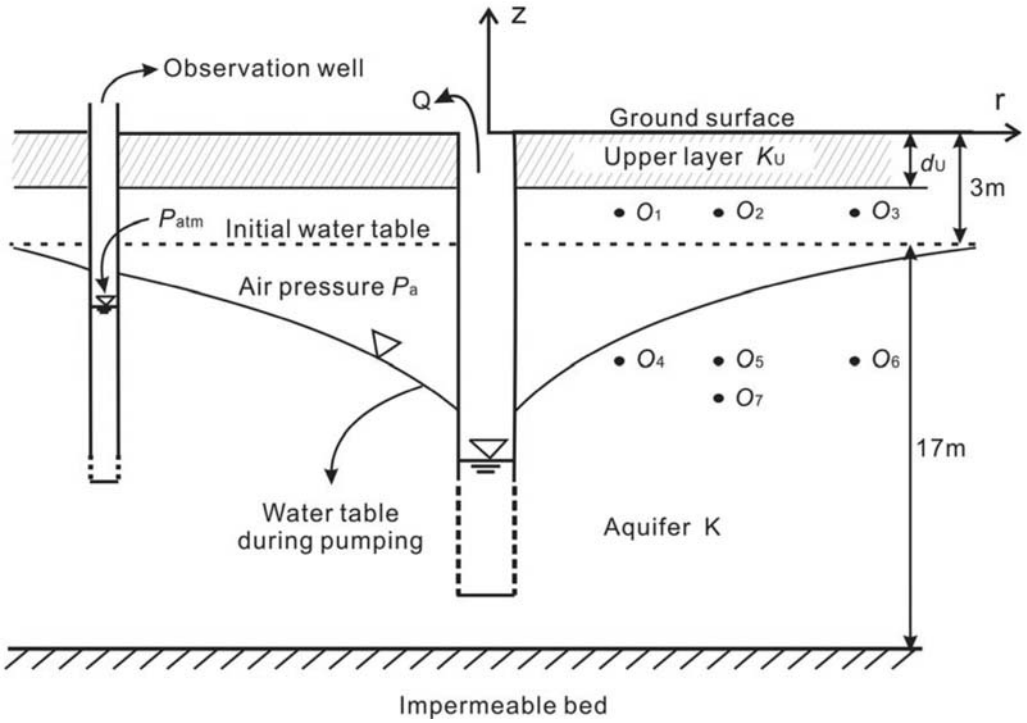

Figure 1. Schematic model domain indicating the geometry and boundary conditions used in the test problem.

2.2. Governing Equations

[10] The mathematical model describing two-phase air-water flow is based on the mass balance equation [*Pruess et al.*, 1999],

$$\frac{d}{dt}\int_{V_n} M^\kappa dV_n = \int_{\Gamma_n} \mathbf{F}^\kappa \bullet \mathbf{n}\, d\Gamma_n + \int_{V_n} q^\kappa dV_n. \tag{1}$$

[11] The integration is over an arbitrary subdomain V_n of the flow system under investigation, which is bounded by a closed surface Γ_n. The quantity M appearing in the accumulation term (left hand side) represents mass per volume, with κ labeling the mass component of air or water. $\mathbf{F}$ denotes mass flux and q denotes sinks and sources. $\mathbf{n}$ is a unit normal vector on surface element $d\Gamma_n$, pointing inward into V_n.

[12] The general form of the mass accumulation term in equation (1) can be written in the form

$$M^\kappa = \phi \sum_\beta S_\beta \rho_\beta X_\beta^\kappa \tag{2}$$

[13] The total mass of component κ (air or water) is obtained by summing over the fluid phases β (liquid or gas). ϕ is porosity, S_β is the saturation of phase β (i.e., the fraction of pore volume occupied by phase β), ρ_β is the density of phase β, and X_β^κ is the mass fraction of component κ present in phase β.

[14] Advective mass flux of a component (air or water) is a sum over phases, which can be written as

$$\mathbf{F}^\kappa = \sum_\beta X_\beta^\kappa \mathbf{F}_\beta \tag{3}$$

Individual phase fluxes are given by a multiphase version of Darcy's law:

$$\mathbf{F}_\beta = \rho_\beta \mathbf{u}_\beta = -k \frac{k_{r\beta}\rho_\beta}{\mu_\beta}\left(\nabla P_\beta - \rho_\beta \mathbf{g}\right) \tag{4}$$

[15] Here $\mathbf{u}_\beta$ is the Darcy velocity (volume flux) in phase β; k is absolute permeability; $k_{r\beta}$ is relative permeability to phase β; μ_β is viscosity; P_β is the fluid pressure in phase β; and $\mathbf{g}$ is the vector of gravitational acceleration. The

Table 1. Primary Parameter Values Used in the Base Case of the Numerical Simulation

	Hydraulic Conductivity (m/s)	Pore Compressibility (Pa^{-1})	Porosity ϕ (cm^3/cm^3)	Relative Permeability and Capillary Pressure			
Upper layer	5.54×10^{-8} (K_U)	10^{-7}	0.4	*van Genuchten* [1980]			
				S_{ls} (cm^3/cm^3)	S_{lr} (cm^3/cm^3)	n	α (m^{-1})
				0.902	0.175	1.09	0.5
Aquifer	7.07×10^{-4} (K)	10^{-8}	0.3	Linear function			
				S_{ls} (cm^3/cm^3)	S_{lr} (cm^3/cm^3)	P_C (cm water)	
				1.0	0.21	100	

Table 2. Detailed Locations of the Observation Points

Observation Point	x (m)	z (m)
O_1	20.4	−2.7
O_2	31.8	−2.7
O_3	54.1	−2.7
O_4	20.4	−4.5
O_5	31.8	−4.5
O_6	54.1	−4.5
O_7	31.8	−4.7

pressures in liquid phase (P_l) and gas phase (P_g) are related via the capillary pressure, P_{cap},

$$P_l = P_g + P_{cap} \tag{5}$$

2.3. Soil Parameters for the Base Case

2.3.1. Soil Parameters for the Upper Layer

[16] The capillary pressure P_{cap} of the low-permeability upper layer is described by the van Genuchten function [*van Genuchten*, 1980]

$$P_{cap} = -P_0\left([S^*]^{-1/\lambda} - 1\right)^{1-\lambda} \quad \left(-P_{\max} \le P_{cap} \le 0\right) \tag{6}$$

where λ is a fitting parameter, $S^* = (S_l - S_{lr})/(S_{ls} - S_{lr})$, S_l is water saturation, S_{lr} is residual water saturation, and S_{ls} is saturated water saturation. $P_0 = \rho_w g/\alpha$, ρ_w is density of water, g is the gravitational constant, and α is a fitting parameter.

[17] The van Genuchten-Mualem model [*Mualem*, 1976; *van Genuchten*, 1980] is used to simulate the liquid relative permeability k_{rl} of the upper layer

$$k_{rl} = \begin{cases} \sqrt{S^*}\left\{1 - \left(1 - [S^*]^{1/\lambda}\right)^{\lambda}\right\}^2 & (S_l < S_{ls}) \\ 1 & (S_l \ge S_{ls}). \end{cases} \tag{7}$$

[18] The gas relative permeability k_{rg} is chosen as one of the following two forms [*Pruess et al.*, 1999]

$$k_{rg} = \begin{cases} 1 - k_{rl} & (S_{gr} = 0) \\ \left(1 - \widehat{S}\right)^2\left(1 - \widehat{S}^2\right) & (S_{gr} > 0). \end{cases} \tag{8}$$

with $\widehat{S} = (S_l - S_{lr})/(1 - S_{lr} - S_{gr})$, and S_{gr} is residual gas saturation.

[19] The soil parameters used in the base case are those for a silty clay. Table 1 lists the hydraulic conductivity K_U, the residual and saturated water saturations S_{lr} and S_{ls}, the porosityϕ and the van Genuchten water retention parameters n and α for this soil texture. These data are from the works of *Carsel and Parrish* [1988] and *Wang et al.* [1997]. Similar data sets were used by, for example, *van Genuchten et al.* [1991] and *Schaap et al.* [1998].

2.3.2. Soil Parameters for the Aquifer

[20] Linear functions of relative permeability and capillary pressure are used for the aquifer in the simulation. The relative permeability of liquid phase, k_{rl}, increases linearly from 0 to 1 with the liquid saturation S_l in the range $S_{lr} \le S_l \le 1 - S_{gr}$. The relative permeability of gas phase, k_{rg}, increases from 0 to 1 with the gas saturation S_g in the range $S_{gr} \le S_g \le 1 - S_{lr}$. Here S_{lr} and S_{gr} are the residual saturations of the gas and liquid phases, respectively. Linear capillary pressure function is defined as

$$P_{cap} = \begin{cases} -P_c, & \text{if } S_l \le S_{lr} \\ -P_c\dfrac{1 - S_{gr} - S_l}{1 - S_{gr} - S_{lr}}, & \text{if } S_{lr} < S_l < 1 - S_{gr} \\ 0, & \text{if } S_l \ge 1 - S_{gr} \end{cases} \tag{9}$$

where P_c is the maximum capillary pressure for the soil.

[21] The aquifer parameters (see Table 1) are similar to those used by *Cooley* [1971] and *Neuman* [1972], and the detailed information is also described by *Batu* [1998].

2.4. Numerical Method

[22] The numerical solutions of the air-water two-phase flow are obtained using the EOS3 module in TOUGH2, a general purpose numerical simulator for multi dimensional fluid and heat flow of multiphase, multicomponent fluid mixtures in porous and fractured media. It is assumed that the aquifer system is under isothermal condition (25°C) and the air is approximated as a compressible ideal gas.

[23] A radially symmetric mesh, composed of 9864 cells, is used for the numerical simulation. The vertical mesh sizes are quite fine, ranging from 0.4 m in the saturated zone to 0.01 m at land surface. Horizontal discretization expands logarithmically with mesh sizes ranging from 0.1 m to 50 m.

[24] Seven observation points are selected to discuss the simulation results (Figure 1) and their exact positions are shown in Table 2. The observation points O_1, O_2 and O_3 in the unsaturated zone is selected to discuss change of the air pressure induced by pumping. The points O_4, O_5, O_6 and O_7 are selected to discuss how hydraulic heads in the aquifer change in response to water pumping.

3. Analysis and Discussion of the Simulation Results for the Base Case

[25] Water table is commonly defined as the surface on which the fluid pressure in the pores of a porous medium is exactly atmospheric [*Fetter*, 1994; *Freeze and Cherry*, 1979]. However, this definition does not apply in this study because the air pressure in the unsaturated zone may be below zero. The water table is then defined as the boundary between unsaturated and the saturated zone [*Fetter*, 1994]. In the case that the air pressure (P_a in Figure 1) in the unsaturated zone is lower than the atmospheric pressure, the water level in the shallow well will be lower than the water table because the piezometer is open to the atmosphere. During the pumping test, the drawdown is defined as the decline of water level in the piezometer, reflecting the decrease of fluid pressure at the observation point.

3.1. Pumping-Induced Air Pressure in Unsaturated Zone

[26] Prior to pumping, the initial air pressure in the unsaturated zone is equal to the atmospheric pressure. Figure 2 shows the air pressure at point O1, O2 and O3 in the unsaturated zone in response to pumping. When the water table drops, negative pressures are created. This is because extra pore space is formed when water table falls,

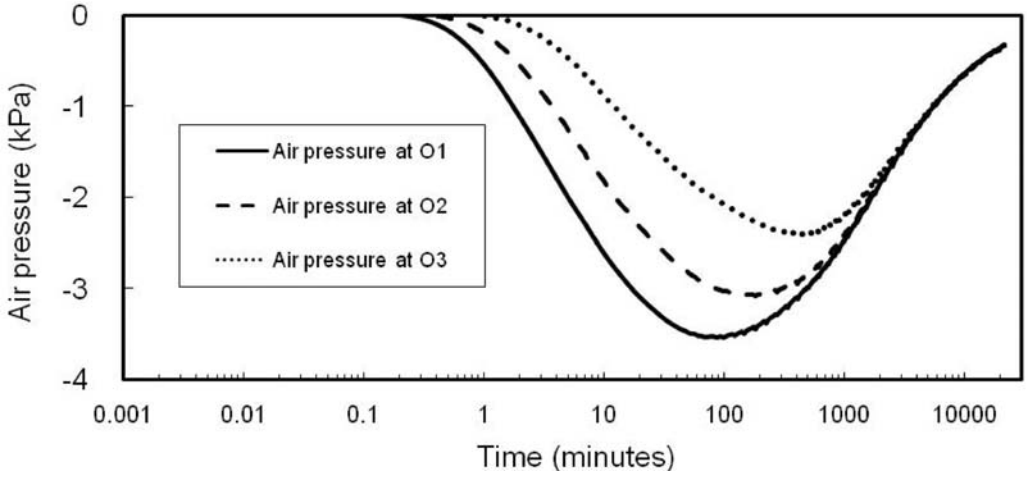

Figure 2. Change of air pressure at O1, O2, and O3 with time for the base case.

the negative pressure is enhanced when the low-permeability surface prevents the air entry from the atmosphere to fill the extra pore space.

[27] The air pressure-time curves are bell shaped: the pressure decreases from zero to a peak value (hereafter defined as P_{max}), and then increases gradually until reaching the initial air pressure prior to pumping. As expected, the peak value is smaller and the time to achieve it is longer as the radial distance increases.

[28] Figure 3 shows the relation between air pressure, drawdown, and drawdown rate at O1. There does not appear to be a clear relation between air pressure and drawdown, but the relation between the air pressure and drawndown rate is obvious: the negative pressure begins to appear when the drawdown rate is approaching its peak, gradually decreases to P_{max} when the drawdown rate remains greater than zero, or the water level continues to fall appreciably. This observation is similar to the conclusion that tide-induced air pressure in coastal aquifer is closely related to the fluctuation rate of the water level [*Jiao and Li*, 2004; *Guo and Jiao*, 2008]. When the system approaches a so-called quasisteady state and the drawdown does not increase much with time any more, or the drawdown rate is almost zero, the air pressure begins to recover and gradually it drops to zero.

3.2. Pumping-Induced Air Pressure and Its Impact on Drawdown and Water Table

[29] The numerical model is run first to reproduce the S-shaped time-drawdown curves in a uniform unconfined aquifer. In this case, the subsurface system is air-unconfined and pumping-induced air pressure is expected to be negligible. Then the hydraulic conductivity of the shallow zone of 2.4 m thick is given a much lower value and the model is run again under the air-confined condition. The results from the two runs are to be used to investigate pumping-induced airflow and its possible impact on drawdown and water table in the aquifer.

[30] Figure 4 shows the simulation results with and without the lower-permeability cap. As expected, when the subsurface system is uniform, the pumping-induced air pressure is almost zero and the drawdown versus time curve shows the typical S shape. Also, there is almost no visual

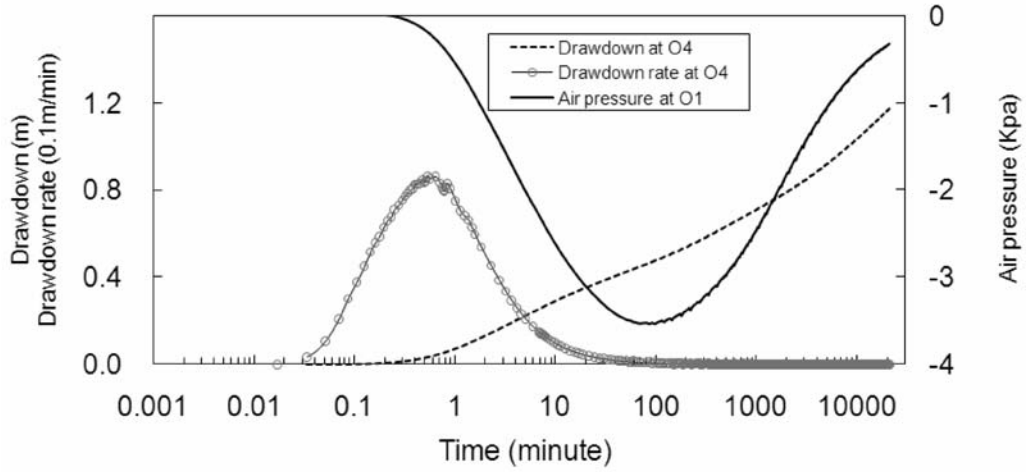

Figure 3. Change of air pressure, drawdown, and drawdown rate with time at O1 for the base case.

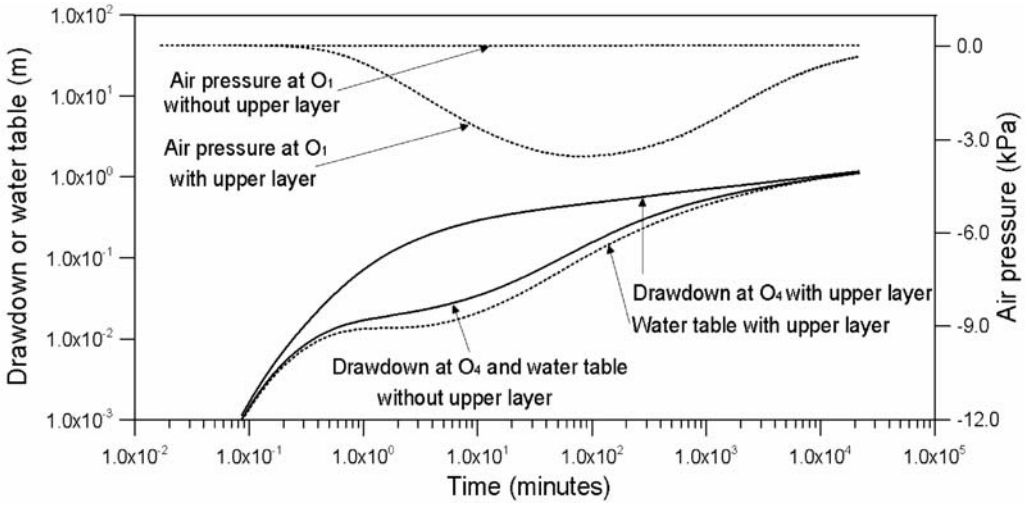

Figure 4. Time evolution of air pressure at O1, drawdown, and water table at O4.

difference between the drawdown and the water table versus time curves and they can be expressed almost by the same line.

[31] When the shallow zone is given a much lower permeability, the negative air pressure occurs. For the base case, at time = 99 min, P_{max} of −3.54 kPa is achieved, which is equivalent to a water column of 0.36 m. This is very significant considering the fact that the drawdown at O4 at this moment is only 0.48 m. This significant negative air pressure may have important impact on the characteristic of the drawdown and water table versus time curves.

[32] During the pumping, there will be a decline in storage, accompanied by a corresponding decline in water levels in piezometers. If negative pressure above the water table is developed, there will be an additional decline in water levels in the piezometers (Figure 1). Therefore the water level in piezometers will drop more quickly when negative pressure is generated due to the low-permeability cap compared to the case without the cap. The water table in the aquifer, however, declines more slowly due to vacuum or suction above the water table. As shown in Figure 4, the water table decrease at x = 20.4 m is less than the drawdown at point O_4. Due to impact of airflow, the drawdown versus time curve at O_4 is similar to that of a confined aquifer and the intermediate flat segment has become unapparent.

[33] When the soil above the water table is uniformly air permeable, the air pressure induced by pumping is negligible (Figure 4). In this case, the drawdown-time curve calculated from the numerical simulation is very similar to that from a traditional analytical model for unconfined aquifers and is S shape. When the low-permeability cap is presented and negative air pressure is developed, water in the pores in the unsaturated zone is sucked by the negative pressure, the gravity drainage from the pores in the unsaturated zone is reduced. Consequently, the drawdown obtained from the air-confined aquifer is much greater than that calculated from the model without the low-permeability cap. So the drawdown versus time curve may not conform to the traditional S-shaped curve for an unconfined aquifer. The intermediate flat segment of the curve formed by the recharge effect of gravity drainage almost disappears and the drawdown behavior is close to that of a confined aquifer.

[34] For the specific example shown in Figure 4, the difference in drawdown between the cases with and without the upper layer is very obvious during 0.2 and 1000 min and the maximum difference is 0.33 m at time equal about 60 min. Such a difference in the drawdown computed from these two cases indicates the impact of airflow on drawdown prediction. For this example, if the low-permeability cap is ignored and the airflow is not considered, the maximum relative error in the estimated drawdown occurs at time = 6.8 min. At this time, drawdowns from the models with and without the cap are 0.253 and 0.028 m, respectively, and the absolute relative error is $|0.252 - 0.028|/0.252 = 88\%$.

3.3. Impact of Airflow on Drawdown With Radial Distance

[35] Figure 5 shows the variation of the air pressure and the drawdown with radial distance from the pumping well. When the subsurface system is uniform or the low-permeability cap does not occur, the drawdown-time curves depict the typical S shape. With increasing radial distance from the well, the effect of elastic storage decreases and the intermediate flat segment at the curves become unapparent. For the same time, the drawdown, as expected, decreases with the radial distance. The air pressure in the unsaturated zone remains a minor value during the whole period of pumping because the good connection between air in the soil and in the atmosphere.

[36] When there is a low-permeability cap, significant negative air pressures can be induced in the unsaturated zone. Like the drawdown of the hydraulic head in the aquifer, pumping-induced negative air pressures attenuate with radial distance from the pumping well. Figure 5 shows the temporal variation of air pressure at O1, O2, and O3, which are 20.4, 31.8 and 54.1 m away from the pumping well, respectively. The maximum negative air pressures P_{max} at O1, O2, and O3 are −3.54, −3.07 and −2.4 kPa, respectively. P_{max} will be lower and the time to reach P_{max} will be longer as the observation point is farther from the

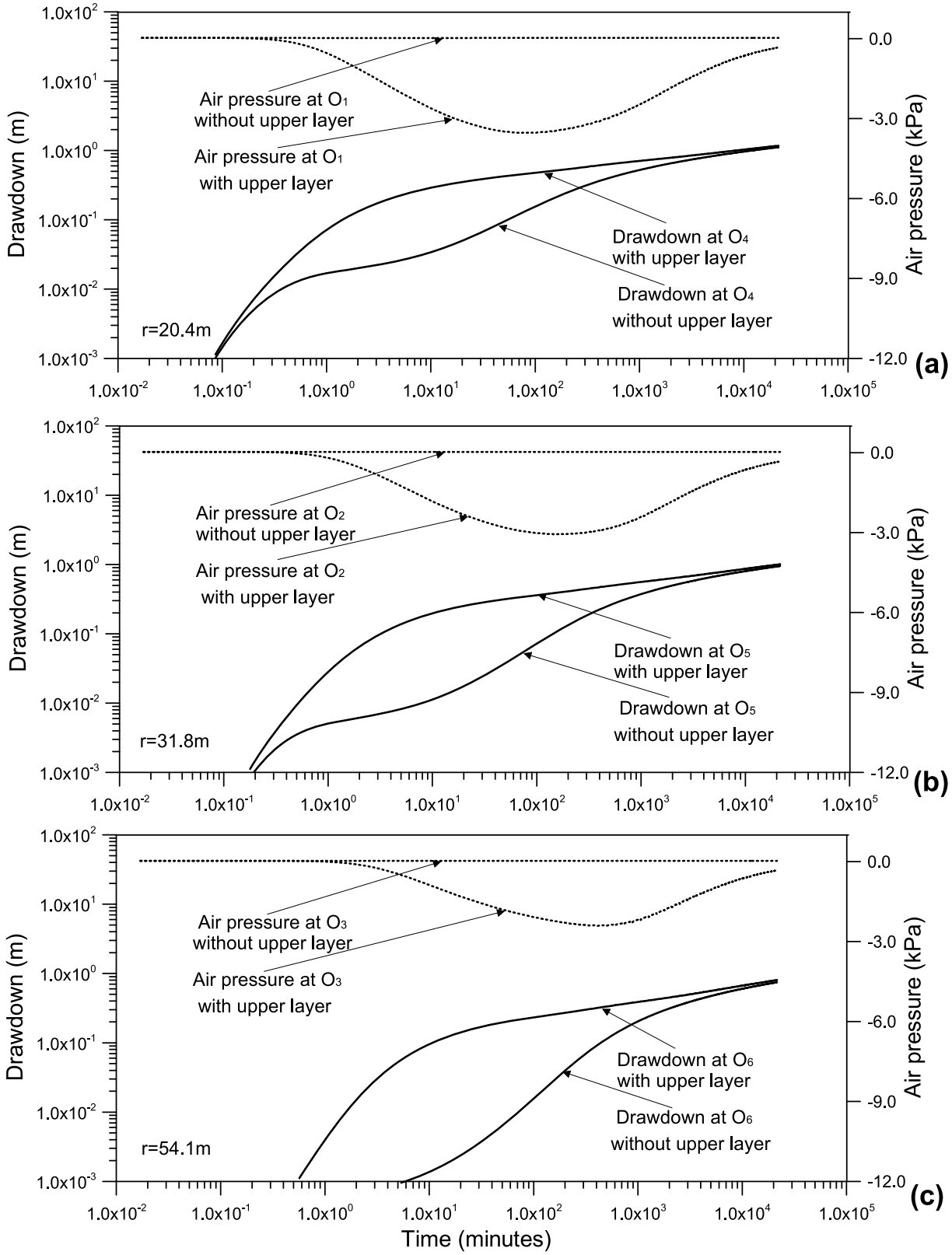

Figure 5. Changes of air pressures with time at three observation points in the unsaturated zone, (a) O1, (b) O2, and (c) O3, and drawdowns at three points in the aquifer, (a) O4, (b) O5, and (c) O6.

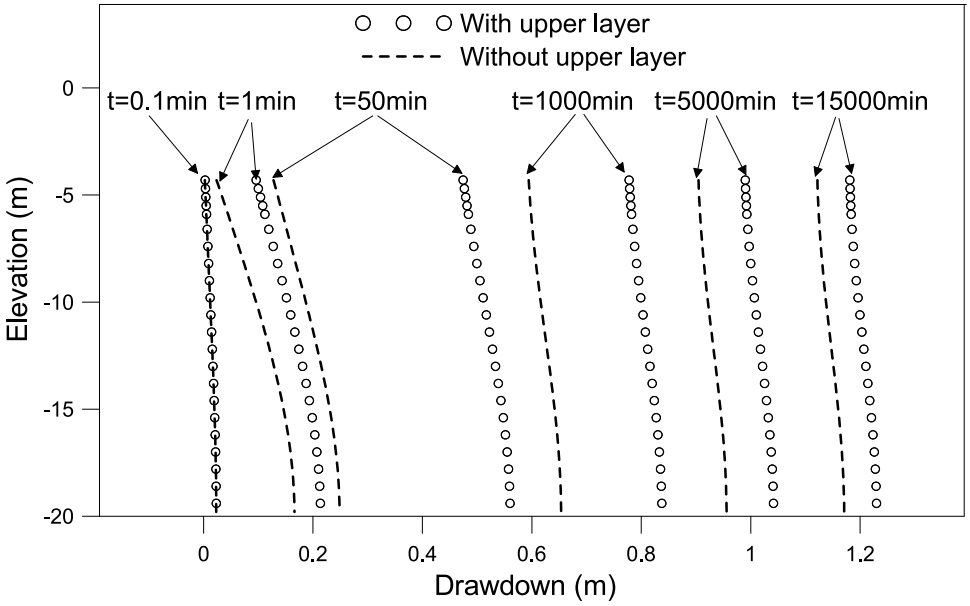

Figure 6. Changes of the drawdown with elevation with r = 16.2 m when the time is 0.1, 1, 50, 1000, 5000, and 15,000 minutes, respectively.

pumping well. The intermediate flat segment of the drawdown versus time curves tends to be unapparent due to impact of the negative air pressures above the water table.

3.4. Impact of Pumping-Induced Airflow on Drawdown With Elevation

[37] Figure 6 shows how the drawdown at a radial distance of 16.2 m changes with elevation at different times. When t = 0.1 min, the curves are almost vertical, indicating the water flows almost horizontally to the well. In the intermediate phase, the drawdown close to the water table is less than the drawdown at greater depths, which indicates significant vertical flow. This is because of gravity drainage, i.e., the water body in the cone of depression contributes water to the water table so that the drawdown increases slowly. As time increases, the drawdown versus elevation curves again become almost vertical, meaning that again water flows mainly horizontally to the well.

[38] As shown in Figure 6, the drawdown can be greatly impacted by airflow above the water table so that the drawdown is significantly increased. As discussed previously (Figure 4), the drawdown difference between the cases with and without the upper layer increases with time until reaching a maximum, and then decreases gradually. With t = 0.1 min, there is almost no drawdown difference (Figure 6). With t = 50 min, the drawdown difference reaches a maximum of about 0.35 m at z = −4.3 m. After

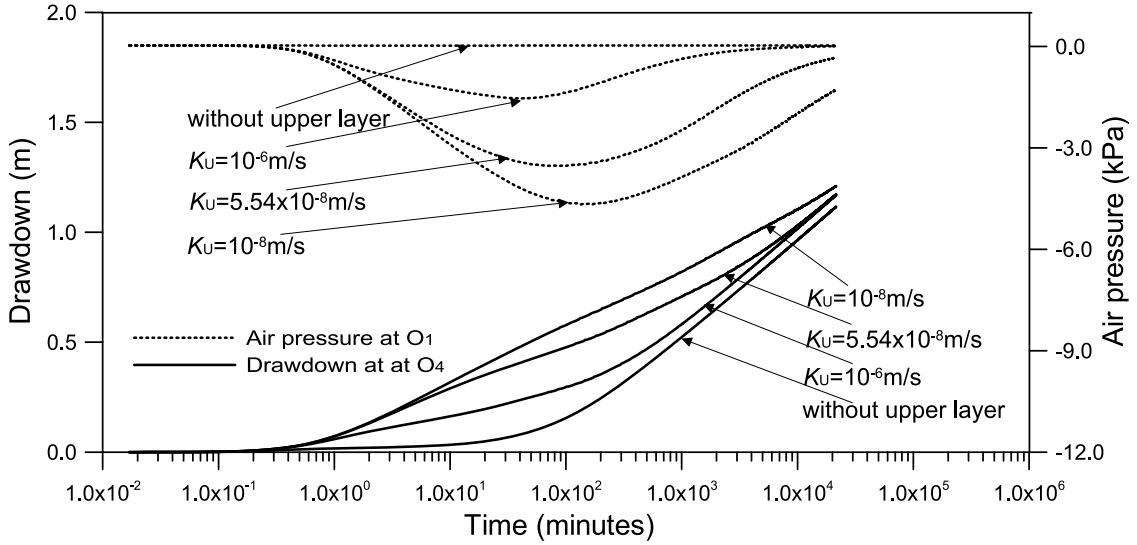

Figure 7. Air pressures at O1 and the drawdown at O4 for different hydraulic conductivities (K_U) of the upper layer.

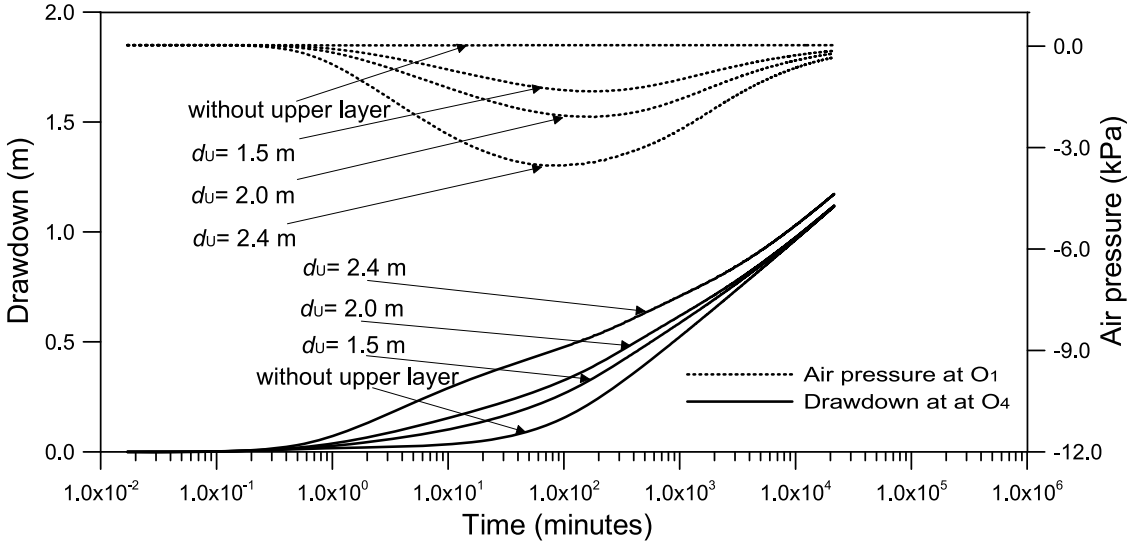

Figure 8. Simulation results of the air pressure at O1 and the drawdown at O4 for different thickness (d_U) of the upper layer.

that, the drawdown difference decreases gradually with time.

[39] When t = 1 min and 50 min, the drawdown difference increases when the observation point becomes closer to the water table. Figure 6 also shows that the decrease of drawdown with elevation in the intermediate phase (e.g., t = 1 and 50 min) becomes more unapparent in the case the low-permeability cap exists compared with the case without the cap. This is because the area close to the water table is more significantly impacted by the negative air pressure.

4. Sensitivity Analysis of Pumping-Induced Airflow and Its Impact on Drawdown in the Aquifer

[40] In this section, sensitivity of pumping-induced airflow and its impact on drawdown in the aquifer predicted by the variably saturated model to the hydraulic conductivity and thickness of the upper layer and the pumping rate are analyzed.

4.1. Sensitivity to Permeability of the Upper Layer K_U

[41] Figure 7 shows how the air pressure at O1 in the unsaturated zone and drawdown at O4 in the aquifer change with time for different values of K_U: Both the maximum negative air pressure P_{max} in the unsaturated zone, and the drawdown in the aquifer decrease with K_U. When $K_U = 1 \times 10^{-8}$, 5.54×10^{-8}, and 1×10^{-6} m/s, the corresponding P_{max} is −4.68, −3.54 and −1.54 kPa, indicating that the parameter K_U has a significant effect on the magnitude of pumping-induced airflow above the water table. Figure 7 also shows that the negative pressure reaches P_{max} later as K_U decreases.

[42] As pumping goes on, the water table drops; at the same time, air in the atmosphere cannot enter the soil freely due to existence of the low-permeability upper layer. Thus negative air pressures form above the water table, which may increase the drawdown in the aquifer. It is expected that the pumping-induced negative air pressure increases when the permeability of the upper layer decreases. As a result, the drawdown in the aquifer increases more significantly when K_U becomes lower. With $k_U = 1 \times 10^{-8}$ m/s, the drawdown at O4 increases so quickly with time that the flat portion of the drawdown versus time curve, formed due to gravity drainage, almost disappears.

4.2. Sensitivity to Thickness of the Upper Layer d_U

[43] The thickness of the low-permeability upper layer d_U is directly related to exchange between air in the atmosphere and in the soil. Figure 8 shows that both the air pressure in the unsaturated zone and the drawdown in the aquifer increase with d_U . The d_U values of 1.5, 2.0, and 2.4 m result in P_{max} values of −1.34, −2.1 and −3.54 kPa, respectively. When d_U increases, the air cannot enter the unsaturated zone freely as water table drops during pumping, thereby leading to greater negative air pressures above the water table. As discussed previously, this negative pressure can increase the drawdown in the aquifer, and therefore change the shape of the drawdown versus time curve. As shown in Figure 8, the flat portion of the drawdown versus time curves becomes more unapparent as d_U increases. With d_U = 2.4 m, the flat portion almost disappears and the shape of the drawdown versus time curve is very similar to that of a confined aquifer. In this case, the behavior of an unconfined aquifer may be mistaken as that of a confined aquifer.

4.3. Sensitivity to Pumping Rate Q

[44] Figure 9 shows temporal changes of the air pressure in the unsaturated zone and the drawdown in the aquifer for different pumping rates. As expected, the pressure decreases and drawdown increases dramatically with increasing pumping rate. During pumping, the low-permeability upper layer impedes air inflow to the soil as water table drops, so that negative air pressures are induced. When pumping rate is great, water table drops quickly, leading to an increase in negative air pressures above the water table. When the pumping rate is 2000 m^3/day, P_{max} is −2.83 kPa. In comparison, P_{max} for pumping rates of 2500 m^3/day and 3000 m^3/day are −3.54 kPa and −4.26 kPa, respectively.

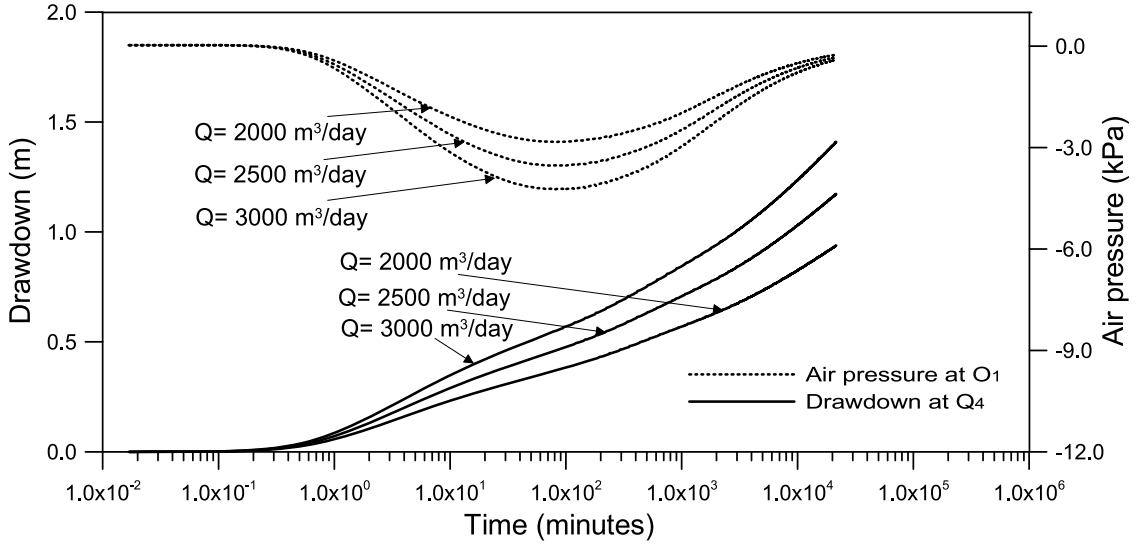

Figure 9. Simulation results of the air pressure at O1 and the drawdown at O4 for different discharge rate (Q) of the pumping well.

4.4. Sensitivity to Aquifer Anisotropy

[45] In the previous discussion, it is assumed that the aquifer is homogeneous and isotropic, i.e., $K_z = K_r = K$, where K_z and K_r represent the vertical and horizontal hydraulic conductivities of the aquifer, respectively. In reality, however, sedimentary aquifers typically exhibit anisotropy in hydraulic conductivity and the ratio K_z/K_r often ranges between 0.01 and 0.1. Figure 10 shows temporal changes of the air pressure in the unsaturated zone and the drawdown in the aquifer for different ratios of K_z/K_r when K_r is fixed at 7.07×10^{-4} m/s. As expected, both the negative air pressure and the drawdown decrease with decreasing K_z/K_r. When the ratio of K_z/K_r becomes low, the vertical component of the water velocity decreases, the contribution of the vertical flow decreases accordingly when the pumping rate of the well remains unchanged. As a result, a smaller drawdown rate is induced in the aquifer, which then leads to smaller negative air pressure in the unsaturated zone.

5. Impact of Pumping-Induced Airflow on Parameter Estimation

[46] The low-permeability upper layer, which is ignored in traditional pumping tests, may lead to negative air pressures in the unsaturated zone and therefore impact the drawdown in the aquifer especially in the early period of pumping. Thus using the observation data obtained from the early period for parameter estimation may lead to erroneous results. However, the impact of airflow on the drawdown is expected to become unsignificant in the late period of pumping when the drawdown rate is minor. As shown in Figure 2, the drawdown difference with and without upper layer has become very small in the late time of pumping.

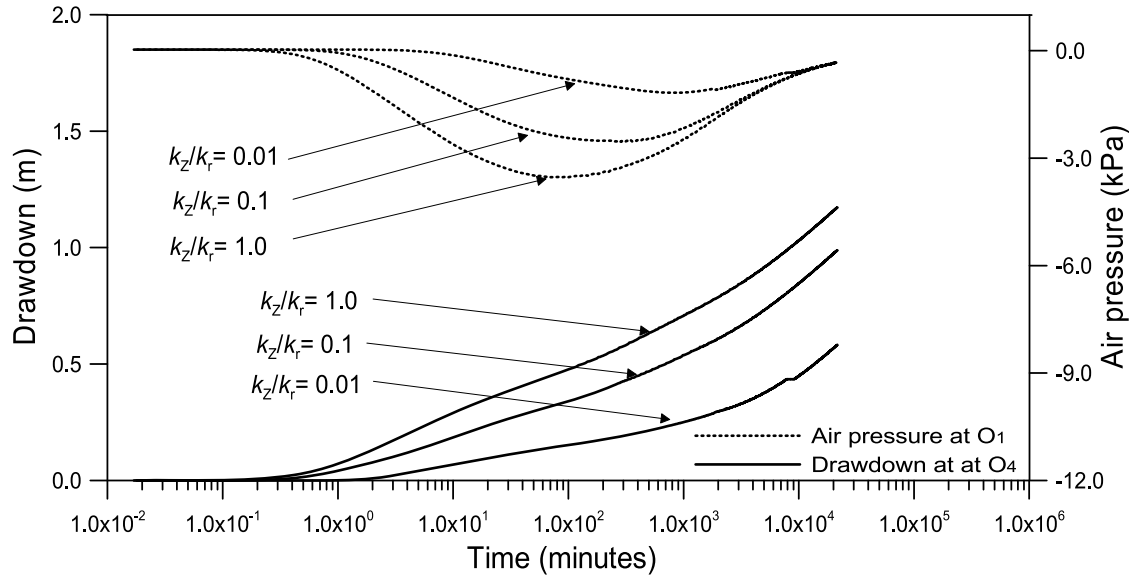

Figure 10. Air pressure at O1 and drawdown at O4 for different K_z/K_r ratios of the aquifer.

Table 3. Impact of Airflow on Parameter Estimation When Airflow is Ignored (Q = 2500 m^3/day)

	True Parameters				Estimated Parameters			
Aquifer Systems	d_U (m)	K_U (m/s)	K (m/s)	S_y	K_e (m/s)	$(K_e - K)/K$ (%)	S_{y_e}	$(S_{y\_e} - S_y)/S_y$ (%)
1 (Base case)	2.4 m	5.54e−08	7.07e−04	0.24	8.13e−04	14.9	0.1	−58.8
2	1.5 m	5.54e−08	7.07e−04	0.24	7.76e−04	9.7	0.17	−30.0
3	2.0 m	5.54e−08	7.07e−04	0.24	8.04e−04	13.7	0.14	−40.1
4	2.4 m	1.00e−08	7.07e−04	0.24	1.12e−03	58.3	0.01	−95.7
5	2.4 m	1.00e−06	7.07e−04	0.24	7.23e−04	2.2	0.17	−28.7

Therefore the drawdown versus time data in this period may be used to estimate the aquifer parameters. In this section, we will discuss the possible errors between the true and estimated aquifer parameters computed from the late time observed drawdown data using the *Neuman* [1974] partially penetrating wells model.

[47] The "true values" of the aquifer parameters denote the parameters used in the simulation. Then the aquifer parameters are estimated with drawdown versus time curves at point O7 (Figure 1). By comparing the "estimated" and "true" values of the parameters K and S_y, one can see the parameter estimation errors caused by the airflow.

[48] The true and estimated parameters as well as their relative errors are listed in the Table 3. Overall, the hydraulic conductivity of the aquifer (K) is overestimated and the specific yield of the aquifer (S_y) is underestimated. The estimation errors for S_y tends to be greater than the errors for K. The errors for the estimated parameters can be great if the impact of airflow on the drawdown is ignored. With $k_U = 1 \times 10^{-8}$ m^2, d_U = 2.4 m (case 4 in Table 3), K is overestimated by 58.3% and S_y underestimated by 95.7%. For the other cases, the estimation errors for K are less than 20%, and estimation errors for S_y are more than 30% except case 5. The estimation errors for values of hydraulic conductivity appear to be not too great if late time observed drawdown data are used for the estimation with the traditional model without considering airflow. However, the specific yield S_y may be greatly underestimated even estimated with late time observation data.

[49] The results in Table 3 also indicate that the estimation errors increase with d_U and decreases with k_U. This is readily understood because pumping-induced negative air pressures become greater as d_U increases and k_U decreases.

6. Summary and Conclusions

[50] Since the 1930s, many analytical and numerical models of transient flow to wells have been developed to interpret the test data. These models, however, focus mainly on single-phase water flow in saturated aquifers. For the first time, an air-water two-phase numerical model is presented to investigate pumping-induced airflow and its possible impact on the drawdown in the aquifer with a low-permeability upper layer on the top.

[51] An aquifer is air-confined when there is a low-permeability layer on the top. Pumping in an air-confined aquifer may lead to significant negative air pressures in the unsaturated zone, as compared to the total drawdown in the aquifer. The negative pressure begins to appear as the drawndown rate increases to a maximum and approaches a maximum when the drawdown rate becomes zero. After that, the negative pressure will gradually drop to zero and the pressure in the unsaturated zone will return to atmospheric pressure. The negative pressure becomes more significant when the permeability of the cap becomes lower or the pumping rate is greater.

[52] The water table appears to be held by the negative pressure and drops more slowly than the case without the low-permeability cap. Because the water in the pores in the unsaturated zone is sucked by the negative pressure, the gravity drainage from the pores in the unsaturated zone is hampered. Consequently, the drawdown obtained from the air-confined aquifer is much greater than that calculated from the model without the low-permeability upper layer. The drawdown versus time curve may not conform to the traditional S-shape curve for an unconfined aquifer. The intermediate flat segment of the curve formed by the recharge effect of gravity drainage becomes unapparent and the drawdown behavior is close to that of a confined aquifer. The drawdown difference between the cases with and without the low-permeability upper layer is negligible when pump starts, but increases with time during the period of so-called intermediate flat segment, then disappear again at later stage of the pumping. If the low permeability is ignored, the maximum error in estimated drawdown could be 88%. The study suggests that the layer above water level, which was ignored in traditional pumping test, has impact on test results. If the airflow is ignored in the air-confined aquifer, overall, the hydraulic conductivity of the aquifer is overestimated and the specific yield of the aquifer is underestimated. The estimation errors for specific yield tend to be greater than the errors for hydraulic conductivity. However, the impact of airflow on the drawdown and parameter estimation is nil in the long-term production period when drawdown rate is almost zero or the system approaches a quasisteady state. Cautions should be taken when the behavior and parameters obtained from short-term tests are used for long-term prediction.

[53] A better understanding of the vacuum generated by pumping may also provide insights into the mechanism of the common engineering problem of ground collapse induced by extensive groundwater withdrawal. These will be topics for further study.

[54] **Acknowledgments.** The study was supported by the Research Grants Council of the Hong Kong Special Administrative Region, China (HKU 7028/05P and HKU 701908P). TOUGH2 was run via the interface of PetraSim. The comments from Professor Shlomo Neuman and two anonymous reviewers have led to an improvement of the paper.

References

Batu, V. (1998), *Aquifer Hydraulics: A Comprehensive Guide to Hydrogeologic Data Analysis*, Wiley Interscience, Hoboken, N. J.

Boulton, N. S. (1954), Unsteady radial flow to a pumped well allowing for delayed yield from storage, *IASH Publ.*, *37*, 472–477.

Carsel, R. F., and R. S. Parrish (1988), Developing joint probability distributions of soil water retention characteristics, *Water Resour. Res.*, *24*, 755–769.

Celia, M. A., and P. Binning (1992), A mass conservative numerical solution for 2-phase flow in porous media with application to unsaturated flow, *Water Resour. Res.*, *28*, 2819–2828.

Cooley, R. L. (1971), Finite difference method for unsteady flow in variably saturated porous media: Application to a single pumping well, *Water Resour. Res.*, *7*, 1607–1625.

Endres, A. L., J. P. Jones, and E. A. Bertrand (2007), Pumping-induced vadose zone drainage and storage in an unconfined aquifer: A comparison of analytical model predictions and field measurements, *J. Hydrol.*, *335*(1–2), 207–218.

Fetter, C. W. (1994), *Applied Hydrogeology*, Prentice-Hall, New York.

Freeze, R. A., and J. A. Cherry (1979), *Groundwater*, Prentice-Hall, Englewood Cliffs, N. J.

Guo, H. P., and J. J. Jiao (2008), Numerical study of the airflow in the unsaturated zone induced by sea tides, *Water Resour. Res.*, *44*, W06402, doi:10.1029/2007WR006532.

Guo, H. P., J. J. Jiao, and E. P. Weeks (2008), Rain-induced subsurface airflow and Lisse effect, *Water Resour. Res.*, *44*, W07409, doi:10.1029/2007WR006294.

Jiao, J. J., and H. L. Li (2004), Breathing of coastal vadose zone induced by sea level fluctuations, *Geophys. Res. Lett.*, *31*, L11502, doi:10.1029/2004GL019572.

Li, H. L., and J. J. Jiao (2005), One-dimensional airflow in unsaturated zone induced by periodic water table fluctuation, *Water Resour. Res.*, *41*, W04007, doi:10.1029/2004WR003916.

Linden, D. R., and R. M. Dixon (1973), Infiltration and water table effects of soil air pressure under border irrigation, *Soil Sci. Soc. Am. J.*, *37*, 94–98.

Mathias, S. A., and A. P. Butler (2006), Linearized Richards' equation approach to pumping test analysis in compressible aquifers, *Water Resour. Res.*, *42*, W06408, doi:10.1029/2005WR004680.

Moench, A. F. (1995), Combining the Neuman and Boulton models for flow to a well in an unconfined aquifer, *Ground Water*, *33*(3), 378–384.

Moench, A. F. (2004), Importance of the vadose zone in analyses of unconfined aquifer tests, *Ground Water*, *42*(2), 223–233.

Moench, A. F. (2008), Analytical and numerical analyses of an unconfined aquifer test considering unsaturated zone characteristics, *Water Resour. Res.*, *44*, W06409, doi:10.1029/2006WR005736.

Mualem, Y. (1976), New model for predicting hydraulic conductivity of unsaturated porous-media, *Water Resour. Res.*, *12*, 513–522.

Neuman, S. P. (1972), Theory of flow in unconfined aquifers considering delayed response of the water table, *Water Resour. Res.*, *8*, 1031–1045.

Neuman, S. P. (1974), Effects of partial penetration on flow in unconfined aquifers considering delayed gravity response, *Water Resour. Res.*, *10*, 303–312.

Peck, A. J. (1965), Moisture profile development and air compression during water uptake by bounded bodies: 3. Vertical columns, *Soil Sci.*, *100*, 44–51.

Pruess, K., et al. (1999), *TOUGH2 User's Guide, Version 2.0*, Earth Sci. Div. Lawrence Berkeley Natl. Lab. Univ. of Calif., Berkeley, Calif.

Schaap, M. G., F. J. Leij, and M. T. van Genuchten (1998), Neural network analysis for hierarchical prediction of soil hydraulic properties, *Soil Sci. Soc. Am. J.*, *62*(4), 847–855.

Tartakovsky, G. D., and S. P. Neuman (2007), Three-dimensional saturated-unsaturated flow with axial symmetry to a partially penetrating well in a compressible unconfined aquifer, *Water Resour. Res.*, *43*, W01410, doi:10.1029/2006WR005153.

Theis, C. V. (1935), The relation between the lowering of the piezometric surface and the rate and duration of discharge of a well using groundwater storage, *Am. Geophys. Union Trans.*, *16*, 519–524.

Touma, J., and M. Vauclin (1986), Experimental and numerical analysis of two-phase infiltration in a partially saturated soil, *Transp. Porous Media*, *1*, 27–55.

Touma, J., G. Vachaud, and J.-Y. Parlange (1984), Air and water flow in a sealed, ponded vertical soil column: Experiment and model, *Soil Sci.*, *137*, 181–187.

van Genuchten, M. T. (1980), A closed-form equation for predicting the hydraulic conductivity of unsaturated soils, *Soil Sci. Soc. Am. J.*, *44*, 892–898.

van Genuchten, M. T., F. J. Leij, and S. R. Yates (1991), The RETC code for quantifying the hydraulic functions of unsaturated soils, *Rep. EPA/600/2-91/065*, U.S. Salinity Lab., Riverside, Calif.

Wang, Z., J. Feyen, D. R. Nielsen, and M. T. van Genuchten (1997), Two-phase flow infiltration equations accounting for air entrapment effects, *Water Resour. Res.*, *33*, 2759–2767.

Weeks, E. P. (2002), The Lisse effect revisited, *Ground Water*, *40*, 652–656.

Zurbuchen, B. R., V. A. Zlotnik, and J. J. Butler, Jr. (2002), Dynamic interpretation of slug tests in highly permeable aquifers, *Water Resour. Res.*, *38*(3), 1025, doi:10.1029/2001WR000354.

H. Guo and J. J. Jiao, Department of Earth Sciences, University of Hong Kong, James Lee Science Building, Room 302, Pokfulan Road, Hong Kong, China. (hpguo79@gmail.com; jjiao@hku.hk)